CRYSTAL GROWTH & DESIGN

Article

Cite This: *Cryst. Growth Des.* 2020, 20, 167−177

pubs.acs.org/crystal

Polymorphism of Merocyanine Dyes Homologues with 1,3-Diethyl-2-thiobarbituric Acid Acceptor and *p*-Dimethylaminobenzene Donor and Different Polymethine Chains Connecting Them

Published as part of a Crystal Growth and Design virtual special issue Remembering the Contributions and Life of Prof. Joel Bernstein

Sergei Rigin,[†] John Tillotson,[‡] Joseph Perry,[‡] Victor N. Khrustalev,[†,§] Georgii Bogdanov,[†] and Tatiana V. Timofeeva*[,†]

[†]Department of Chemistry, New Mexico Highlands University, Las Vegas, New Mexico 87701, United States

[‡]School of Chemistry and Biochemistry, Georgia Institute of Technology, Atlanta, Georgia 30332, United States

[§]Peoples' Friendship University of Russia (RUDN University), 117198 Moscow, Russia

Supporting Information

ABSTRACT: The crystallization from different solvents of homologues of 1,3-diethyl-2-thiobarbituric acid and *p*-dimethylaminobenzene with different lengths of the polymethine bridge between donor and acceptor groups (TB[*n*]) produced three pairs of polymorphs with the number of C═C bonds in the chain *n* = 1, 3, and 5. The homologues with the shortest (one methine unit) π-conjugated bridge were presented by two concomitant (obtained simultaneously) polymorphs. Bond length alternation values calculated using X-ray data and evaluation using NMR data showed that some homologues possesses a very high hyperpolarizability. It was shown that the increase of polarizability is related to the increase in the length of the π-conjugated bridge that was supported by experimental hyper-Rayleigh scattering data. Density functional theory calculations of HOMO/LUMO molecular energy levels indicated that compounds with a longer π-conjugated bridge have a higher thermal stability.

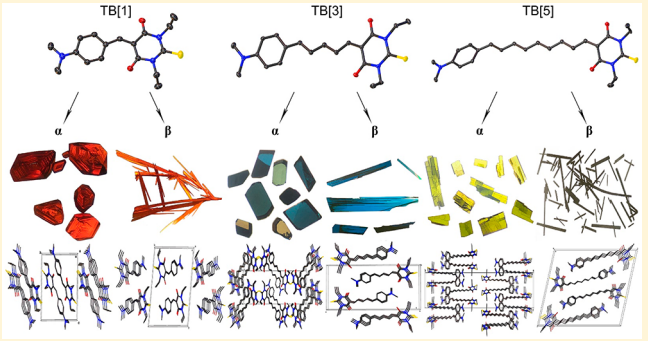

INTRODUCTION

As in many other research groups, studying polymorphism and applications of crystal engineering in our group was to a great extent inspired by Joel Bernstein. In addition to his deep knowledge, huge scientific intuition, and personal charm, our generation of crystallographers was educated from his book *Polymorphism in Molecular Crystals*.[1] Some of us were extremely lucky since Joel Bernstein allowed us to translate and publish his book into Russian.[2] Information collected on phase transitions, crystalline polymorphism, and applications of these phenomena is very wide. On the other hand, even knowing the physical fundamentals of these phenomena, it is still impossible to completely predict polymorphism, since too many factors are involved in formation of new polymorphs, and the crystal energy landscape generated to predict crystal structure gives many possible solutions, and only some of them represent possible polymorphs.[3−5] Because of that, experimental studies of polymorphs of different groups of compounds should be continued for the accumulation of new knowledge as a basis for a stronger correlation between theory and experiment.

In many cases, crystallization from different solvents brings about the formation of different polymorphs.[1,6,7] It is known that variation of molecular positions and/or molecular conformation inside three-dimensional (3D) crystalline space brings significant variation of crystal properties. In the case of pharmaceutically active compounds, it is important to mention the differences in polymorph thermal stability, melting points, solubility, and bioavailability.[8−10] For potential nonlinear optical (NLO) polymorphic materials, thermal stability is also important, but in this case, the molecular packing mode in crystals is more important since only acentric crystals can produce second-order NLO effects.[11−15] The influence of molecular packing in polymorphs on electrical, magnetic, and spectral properties are important for many materials, including charge transfer (CT) materials, that can be used in organic light-emitting diodes (OLEDs), photovoltaic, and biomedical devices.[16−20]

Received: July 19, 2019
Revised: November 21, 2019
Published: December 5, 2019

DOI: 10.1021/acs.cgd.9b00961
Cryst. Growth Des. 2020, 20, 167−177

In this publication, peculiarities of the molecular structure and molecular organization in crystals of several homologues of push−pull molecules with the 1,3-diethyl-2-thiobarbituric group as an acceptor, *p*-dimethylaminophenyl group as a donor, and a polymethine chain with the number of C=C bonds from 1 to 5 are presented. In those materials, thiobarbituric acid groups are strong electron acceptors because they gain aromatic stabilization upon reduction.[21] They can be used along with amine group donors to obtain molecules with high nonlinear optical activity. The search for new organic materials with NLO properties has been of great interest for photonics and optoelectronics for more than four decades. For organic materials to have significant second-order NLO coefficients, they should possess a high concentration of hyperpolarizable chromophores. The great variety of organic chromophore compounds offers exceptional versatility upon design of new materials for NLO application. Organic chromophores should not only have high optical nonlinearities but also possess decent thermal and chemical stability and low optical loss (high transparency).[22] In general, these properties are mutually exclusive. A compromise can be achieved through replacing the aliphatic dialkylamino donor groups with diarylamino groups resulting in a substantial increase in the thermal stability of a wide range of compounds without damaging the nonlinearity of the chromophore. Furthermore, experimental results on thermal stability were explored with computational methods using principal component analysis (PCA).[23] The results demonstrated a strong dependence between thermal stability and HOMO orbital energy: less negative HOMO energy leads to higher thermal stability. Attempts have been made to relate the thermal stability and NLO properties of these compounds with their structure. The quantitative structure−property relationships (QSPR) model was presented to predict decomposition temperature (T_d) values for a diverse set of chromophores using various descriptors such as size, shape, and intramolecular charge.[24] Mean relative error for the prediction was 4.46%, and R^2 of the correlation was 0.9642. The presented model relies solely on descriptors derived from the chemical structure of the molecule and thus is applicable to regular NLO chromophores of any chemical nature.

Many chromophores containing barbituric acid groups have been described in the literature. Among them, a set of organic molecules with huge nonlinearities ($\beta(0)$ up to 911×10^{-30} esu), which are promising building blocks for electro-optic modulator materials, was found.[25] It was demonstrated that derivatives containing diethyl-thiobarbituric group can exhibit very large nonlinearities in comparison to nitro or carbonyl acceptors. Hyperpolarizability values measured in Marder's work were later used as a benchmark for the NLO calculation scheme.[26]

Recently, barbiturate derivatives have been used as organic sensitizers for fabrication of dye-sensitized solar cells.[27] Efficiency of the molecules with barbituric and thiobarbituric acceptors has been compared. It was found that the presented efficiency of these photovoltaic cells was not high. However, it was pointed out that this efficiency might be improved by elimination of molecular aggregation that might be achieved by introduction of long hydrophobic chains in such molecules.

In this paper, synthesis, single crystal X-ray diffraction (except for TB[4]), spectroscopic studies, and DFT calculations of the series of chromophores−thiobarbituric acid derivatives TB[1]−TB[5] (Figure 1) are presented. Crystallization from different solvents allowed us to reveal and describe polymorphism for three homologues: TB[1], TB[3], and TB[5]. Nonlinear optical characteristics of compounds, based on X-ray and NMR data, hyper-Rayleigh scattering, and solvatochromic behavior of these materials are discussed as well.

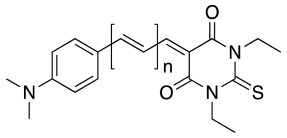

Figure 1. Molecular structure TB[1]−TB[5]: n = 0 for TB[1], n = 1 for TB[2], n = 2 for TB[3], n = 3 for TB[4], and n = 4 for TB[5].

EXPERIMENTAL SECTION

Crystal Growth. All materials and reagents were commercially available and used as received except where noted. Starting aldehydes for the syntheses of TB[1]−TB[5] were prepared as reported in our previous publication.[28] Additional synthesis details are presented in Supporting Information. Crystallizations of samples suitable for X-ray studies have been conducted using several different methods, solvents, and mixtures of solvents with consideration of the solubility of compounds studied.[29] Methods that produced crystals of quality sufficient for X-ray studies are presented below. Single crystals of TB[1] were grown by vapor diffusion of hexane or cyclohexane into a saturated solution of TB[1] in either chloroform or acetone. Additionally, single crystal growth was accomplished by layering ethanol on top of a saturated solution of TB[1] in dichloromethane. The crystal growth took approximately 3 weeks and yielded crystals that were brilliant red in appearance. Single crystals of TB[2] were grown by layering ethanol on top of a saturated solution of TB[2] in dichloromethane. Crystal growth took place over 4−6 weeks and gave lustrous, prism-shaped crystals that were purple and silver in appearance. Single crystals of TB[3] were grown by the slow evaporation of a saturated solution of TB[3] in ethyl acetate (TB[3]α) and layering ethanol on top of a saturated solution of TB[3] in dichloromethane (TB[3]β). Crystal growth took place over 3−4 weeks and gave prism-like, blue and gold crystals (TB[3]α) as well as blue transparent needles (TB[3]β). Single crystals of TB[5] were grown by the slow evaporation of a saturated solution of TB[5] in ethyl acetate (TB[5]α) and layering ethanol on top of a saturated solution of TB[5] in dichloromethane (TB[5]β). Crystal growth took place over 5−6 weeks and gave yellowish-green, plate-like crystals (TB[5]α) as well as black opaque needles (TB[5]β).

X-ray Study. The single-crystal X-ray diffraction data for samples TB[1]α, TB[1]β, TB[2], and TB[3]α were collected on a Bruker SMART APEX II CCD diffractometer (λ(Mo$K\alpha$)-radiation, graphite monochromator, ω and φ scan mode) and corrected for absorption using the SADABS.[30] Sample TB[3]β was analyzed with Rigaku Oxford Diffraction SuperNova, Dual, Cu at home/near diffractometer (λ(Cu$K\alpha$)-radiation, mirror monochromator, ω scan mode) and corrected for absorption using CrysAlisPro.[31] Diffraction data for samples TB[5]α and TB[5]β were collected using Bruker Venture Duo with Photon II diffractometer (λ(Mo$K\alpha$)-radiation, ω and φ scan mode) and corrected for absorption using the SADABS.[30]

For details, see Table 1, Supporting Information. The structures were solved by the intrinsic phasing modification of direct methods,[32] and refined by a full-matrix least-squares technique on F^2 in anisotropic approximation for non-hydrogen atoms. The hydrogen atoms were placed in calculated positions and refined within the riding model with fixed isotropic displacement parameters [U_{iso}(H) = 1.5U_{eq}(C) for the methyl groups and 1.2U_{eq}(C) for the other groups]. All calculations were carried out using the OLEX^2 program suite.[33]

DOI: 10.1021/acs.cgd.9b00961
Cryst. Growth Des. 2020, 20, 167−177

(a) (b) (c)

Figure 2. Photos of the TB[1] samples (α polymorph) obtained using solvent set I (acetone/hexane) (a), set II (dichloromethane/ethanol) (b), and set III (chloroform/cyclohexane) (c).

COMPUTATIONAL METHODS

Computations of molecular geometries, energies, dipole moments and HOMO and LUMO energy levels were carried out at the B3LYP/6-311+G(d, p) level of theory using GAUSSIAN 16 software.[34] For the sake of comparison, two sets of initial coordinates (optimized geometry and X-ray geometry) were used for computations.

Crystal lattice energies (kcal/mol) were calculated using empirical force field approach implemented in the CLP-PIXEL computer program package by A. Gavezzotti (ver. 3.0, available from http://www.angelogavezzotti.it).[35,36] Default force field parameters were used, and the hydrogen atom positions were assigned by the software. Results are presented in Tables S4–S6, Supporting Information.

Spectroscopic Characterization. Linear absorption measurements were performed using either a UV–vis-NIR scanning spectrophotometer (UV-3101PC, Shimadzu). Steady state fluorescence measurements were conducted using a scanning spectrofluorometer (Fluorolog-2, SPEX). All spectra were measured in 1 cm special optical glass cuvettes (SOG, Starna cells).

Hyper-Rayleigh scattering (HRS) measurements were conducted on a home-built Hyper-Rayleigh scattering/two-photon induced fluorescence setup. The light source for the HRS measurements consisted of a Ti:sapphire regenerative amplifier (Solstice, Spectra-Physics, 800 nm, 3.7 W average power, 100 fs pulse width, 1 kHz repetition rate). The amplified laser was used to pump a computer controlled optical parametric amplifier (OPA, TOPAS-C, Light Conversion). The OPA can be continuously tuned from 1100–2600 nm (fwhm 10–30 nm), and the second harmonic of the OPA can be used in the range of 550–1100 nm (~30 mW average power). The range of excitation energy, at the sample, varies between 2–12.5 μJ and is limited below the onset of higher order nonlinear optical effects such as white-light generation. Before entering the sample enclosure, the beam is filtered using appropriate long pass filters (typically 850 nm long pass) to remove stray 800 nm light. The beam then passes through two orthogonally oriented cylindrical lenses and into the sample cell (1 cm path length, Special Optical Glass, Starna Cells). The cell holder was attached to a movable stage allowing the cuvette to be positioned such that the focus of the beam was just next to the wall of the cell, in order to minimize reabsorption. The generated light was collected at a right angle by means of a condensing lens (focal length = 8.0 mm, KPA016-C, Newport Corporation) and was passed through appropriate short pass filters needed to remove scattered light from excitation beam as well as two-photon fluorescence from the sample. The filtered light is collected by fiber collimators (F810SMA-543, Thorlabs) and sent through a two-leg fiber bundle (13 fibers per bundle oriented in a line, Leoni) to an imaging fiber adapter (FC-446-030, Princeton Instruments) that was coupled to a monochromator (SpectrPro-150, Acton). The HRS signal was detected on a liquid nitrogen cooled CCD camera (LN/CCD-1100PB, Roper Scientific, controller: ST-133, Roper Scientific).

For HRS measurements, samples were dissolved in spectroscopy grade solvents at concentrations ranging from 1 μM to 10 mM. HRS spectra were acquired for long exposure times (50–500 s) due to the weak nature of the HRS signal. All samples were stirred with a micro stir bar that was carefully placed below the beam. All hyperpolarizability values were referenced internally to and corrected for the HRS signal and hyperpolarizability of the corresponding solvent.[37] The raw data were processed in MATLAB by first smoothing the data using the built-in smoothing protocol and the robust LOESS function, which was a local regression using a weighted linear least-squares fit with second degree polynomial model and assigns a lower weight to outliers. The smoothing function was adjusted to exclude cosmic rays, typically spanning 0.5–1% of the data. To remove the contribution from multiphoton fluorescence, the baseline of the smoothed data was fit by a fifth-order polynomial using manually selected regions of baseline and subtracted from the raw data.

NMR Study. ^{1}H and ^{13}C NMR spectra were acquired on either a Bruker Avance III HD-500 MHz (with Prodigy cryoprobe) or a Bruker Avance III HD-800 MHz NMR spectrometer. All spectra were referenced internally to their residual solve signal.

RESULTS AND DISCUSSION

Crystal Morphologies. Four different solvent sets (I – acetone/hexane, II – dichloromethane/ethanol, III – chloroform/cyclohexane, IV – chloroform/hexane) were used for sample TB[1] preparation. Crystals of samples I, III, and IV were grown by solvent diffusion, while samples of II were grown by solvent layering. The samples crystallized from solutions I and III had block shapes, while crystals with needle shape were obtained from solution II (Figure 2). Crystals from solution IV had both prism and needle shapes (Figure 3a).

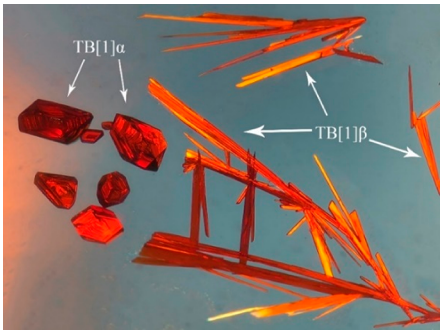

Figure 3. Photo of concomitant polymorphs TB[1]α and TB[1]β obtained using solvent set IV (chloroform/hexane). Calculated crystal morphologies for TB[1]α and TB[1]β along with characteristic crystal shapes photos of polymorphs are presented in Figures S1 and S2, Supporting Information.

Significant differences in morphologies of TB[1] crystals grown from different solvents have been found. Single crystal X-ray diffraction studies performed for each sample have shown that crystals obtained from solutions I–III are, in fact, the same polymorph (TB[1]α) that corresponds to one reported earlier.[27,38] Figure 2 demonstrates that different crystal morphologies (needles and blocks) do not always correspond to different polymorphs. On the contrary, crystals obtained from solution IV (Figure 3) demonstrate two different morphologies that, according to X-ray study, are two concomitant polymorphs TB[1]α and TB[1]β.[39] Crystals

DOI: 10.1021/acs.cgd.9b00961
Cryst. Growth Des. 2020, 20, 167–177

of TB[1]α and TB[1]β possess prism and needle shapes, respectively. Crystal faces of these two polymorphs were calculated using Mercury software[40] (Figures S1 and S2, SI), demonstrating block-like and elongated shape, respectively.

Crystals of TB[2] were obtained by solvent layering of ethanol onto a saturated solution of TB[2] in dichloromethane. The ethanol diffused into the dichloromethane solution over the course of 4−6 weeks, yielding very large prismatic crystals that appeared purple and silver on alternating faces (Figure 4). Only crystals of one form of TB[2] was found

Figure 4. Crystals of TB[2] obtained from dichloromethane/ethanol solution.

suitable to X-ray data. Compound TB[3] gave very thin and long actinic crystals, with almost all solvent systems and crystallization techniques, which were not suitable for X-ray analysis. X-ray quality crystals were finally obtained by very slow evaporation of a saturated solution of TB[3] in ethyl acetate (TB[3]α) and layering ethanol on top of a saturated solution of TB[3] in dichloromethane (TB[3]β). Crystal growth by these methods gave both large, prism-shaped crystals that were blue and gold on alternating faces (TB[3]α) and thin, needle-shaped blue crystals (TB[3]β) (Figure 5).

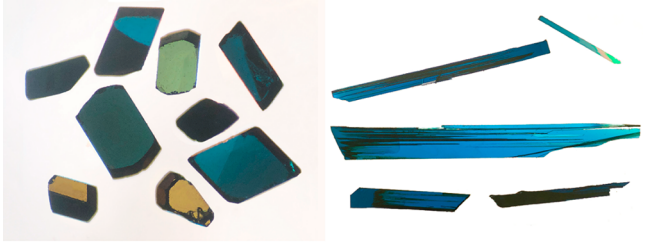

Figure 5. Crystals of TB[3]α and TB[3]β obtained from ethyl acetate solution (a) and ethanol/dichloromethane solution (b). Calculated crystal morphologies for TB[3]α and TB[3]β along with characteristic crystal shape photos of polymorphs are presented in Figures S3 and S4, Supporting Information.

Crystals of TB[2] and TB[3]α were both exceptionally lustrous and almost metallic in appearance. All attempts to crystallize compound TB[4] were unsuccessful. Crystals of TB[5] were obtained by slow evaporation of a saturated solution of TB[5] in ethyl acetate giving yellow-green plates (TB[5]α), and layering ethanol on top of a saturated solution of TB[5] in dichloromethane (TB[5]β) giving thin black needles (TB[5]β) (Figure 6). Calculated crystal faces for polymorphs PB[3] and TB[5] are shown in Figures S3−S6, Supporting Information.

Molecular Structure. Single crystal diffraction studies indicated that molecules in crystals TB[1]α, TB[1]β, TB[2], TB[3]α, and TB[3]β have a nearly planar structure except for ethyl groups. RMS deviations from a plane for molecules are 0.091, 0.111, 0.114, 0.052, and 0.112 Å, respectively. The asymmetric unit of TB[5]α contains two molecules (A and B) with RMS deviations from a plane of 0.350 and 0.344 Å, respectively, and 0.414 Å in TB[5]β (see also Figure S8, Supporting Information). All the above-mentioned data demonstrate that an increase of length of conjugated bridge makes molecules less planar, as it was observed for similar molecules before.[28] The molecules can be divided into three planar fragments that are donor (D), acceptor (A), and π-conjugated bridge (B) (Figure 7). The dihedral angles between these fragments and selected bond lengths for all samples are summarized in Table 2, Supporting Information. This table demonstrates that molecular geometry for all molecules under study does not deviate from standard for this class of compounds. In all molecules, the 4-dimethylamino substituted phenyl ring has quinoid character, and the geometry of the barbiturate fragment corresponds to the keto form (Table 2, Supporting Information, Figure 7). Bond lengths distribution in all molecules demonstrate that extensive molecular polarization occurs in these molecules in the ground state.[35]

It is important to mention that orientations of ethyl substituents are different in all polymorph pairs TB[1], TB[3], and TB[5]. Differences in substituents orientations can be clearly seeing in Figures 8, 9, 10, and 11. It is reasonably to suggest that different molecular conformations have an influence on molecular packing in crystals, so polymorphs presented here can be considered as conformational polymorphs.

Molecular Packing in Crystals. Molecular packings in TB[1]α, TB[1]β, TB[2], TB[5]α, and TB[5]β are defined by the presence of intramolecular C−H···O hydrogen bonds described along with intermolecular H-bonds in Table 3, Supporting Information. Molecule structures, superposition of molecules in different polymorphs, and packing diagrams for TB[1]α,β, TB[2], TB[3]α,β, and TB[5]α,β are presented in Figures 8−11, respectively.

In TB[1]α, molecules are arranged in stacks of parallel molecules along the *a* axis, which form dimers with antiparallel orientation of the molecules, i.e., donor to acceptor and acceptor to donor (Figure 8c) with two symmetrical hydrogen bonds between the molecules (Figure 8e). In the crystal of TB[1]β, molecules form stacks along the *a* axis; the stacks surrounding referenced stack are obtained from it by translations or inversion centers (Figure 8d). Molecules connected through the inversion center have two symmetrical hydrogen bonds between them (Figure 8f). Distances between molecular plains in TB[1]α and TB[1]β are equal to 3.450(4) and 3.545(2) Å respectively, that along with the absence of overlap Ph and barbiturate planar fragments does not suggest $\pi-\pi$ interaction between them.

Molecules in TB[2] are packed in layers parallel to the $(2\bar{1}1)$ plane. Two relatively short contacts C−H···O (2.52 Å) are connecting molecules into centrosymmetric dimers. Overlay of molecular layers brings the formation of molecular stacks along the *b* axis (Figure 9b). Hydrogen bonds for TB[2] are shown in Figure 9c. The thiobarbituric acceptor ring is partially disordered with 85% and 15% fractions of the disordered components. Figures 9a−c show the predominant component only.

DOI: 10.1021/acs.cgd.9b00961
Cryst. Growth Des. 2020, 20, 167−177

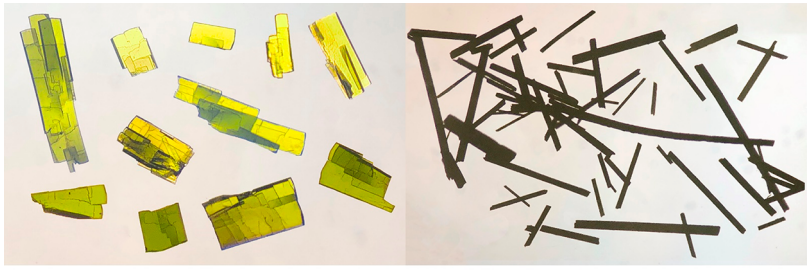

Figure 6. Crystals of TB[5]α and TB[5]β obtained from ethyl acetate solution (a) and ethanol/dichloromethane solution (b). Calculated crystal morphologies for TB[5]α and TB[5]β along with characteristic crystal shapes photos of polymorphs are presented in Figures S5 and S6, Supporting Information.

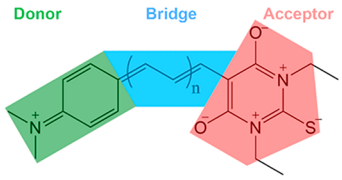

Figure 7. Planar fragments of molecules TB[1]–TB[5].

In the case of TB[3]α, molecules form dimers that are arranged into stacks parallel to the *c* axis, while the stacks form a parquet-like structure (Figure 10c). Hydrogen bonds for TB[3]α are shown in Figure 10e. In TB[3]β, molecules form stacks parallel to the *a* axis (Figure 10d). Hydrogen bonds for TB[3]β are shown in Figure 10f. Dissimilar to polymorphs TB[1]α,β, in polymorph TB[3]α molecular positions, which suggest $\pi-\pi$ interactions between Ph and barbiturate

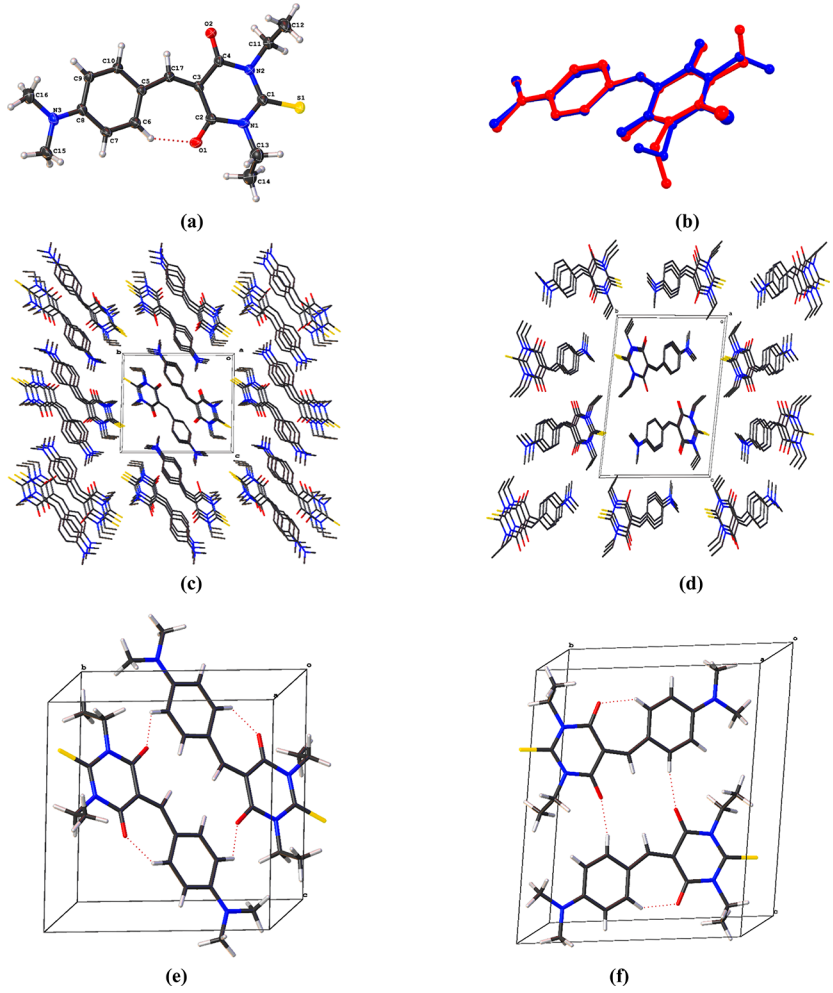

Figure 8. Molecular structure of TB[1]α (a); superposition of TB[1]α (red) and TB[1]β (blue) molecules showing different orientations of the ethyl substituents (b); packing diagram of TB[1]α (c) and TB[1]β (d) along the *a* axis; hydrogen bonds for TB[1]α (e) and TB[1]β (f).

DOI: 10.1021/acs.cgd.9b00961
Cryst. Growth Des. 2020, 20, 167–177

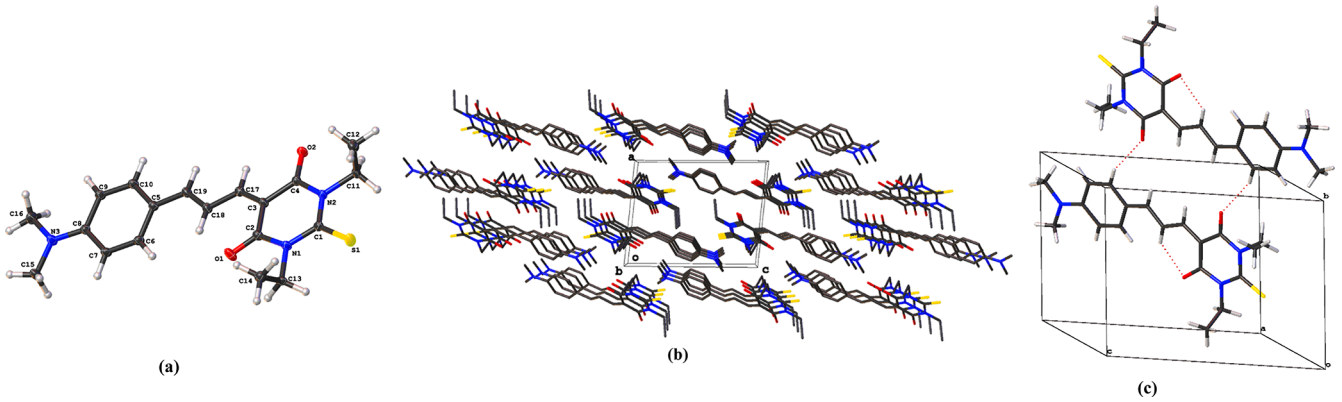

Figure 9. Molecular structure of TB[2] (a), its packing diagram along the *b* axis (b) and hydrogen bonds (c).

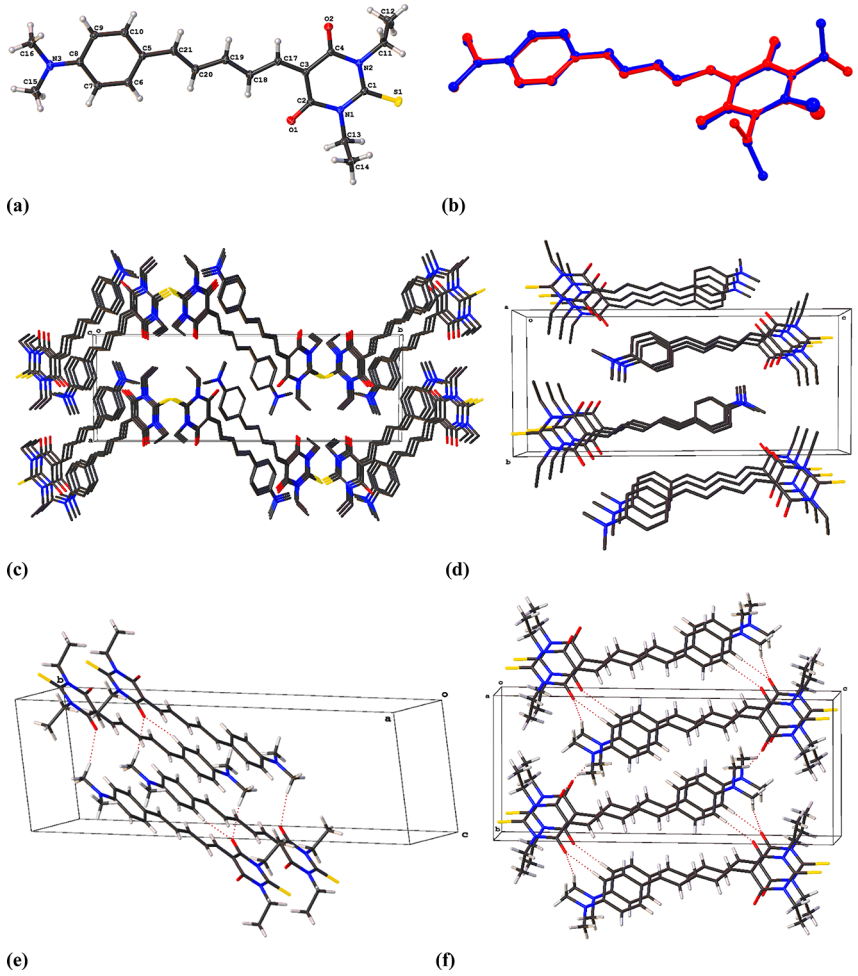

Figure 10. Molecular structure of TB[3]α (a); superposition of TB[3]α (red) and TB[3]β (blue) molecules showing different orientation of the ethyl substituents (b); packing diagram of TB[3]α (c) and TB[3]β (d) along the *c* and *a* axes, respectively; hydrogen bonds for TB[3]α (e) and TB[3]β (f).

substituents, were found (Figure S7, Supporting Information). Such interactions were not observed in the crystal of TB[3]β.

In the case of TB[5]α, two symmetrically independent elongated molecules form stacks that are arranged in pairs with parallel orientation of the molecules within those pairs. The stacks are extended along the *a* axis (Figure 11b). In TB[5]β, stacks are arranged parallel to the *b* axis. A significant difference of molecular conformations in polymorphs TB[5]α and TB[5]β can be seen in Figure S8, Supporting Information. Hydrogen bonds for TB[5]α and TB[5]β are shown in Figure 11, panels d and e, respectively. There is no evidence of stacking infractions in both TB[5] polymorphs. The packing of TB[5]β is similar to that of TB[1]β and TB[3]β. This observation is consistent with the fact that all the presented β-polymorphs have needle-like morphologies.

Relative Polymorphs Stability. On the basis of the obtained data on molecular packing in crystals, lattice energy for all samples studies was calculated using software developed

DOI: 10.1021/acs.cgd.9b00961
Cryst. Growth Des. 2020, 20, 167−177

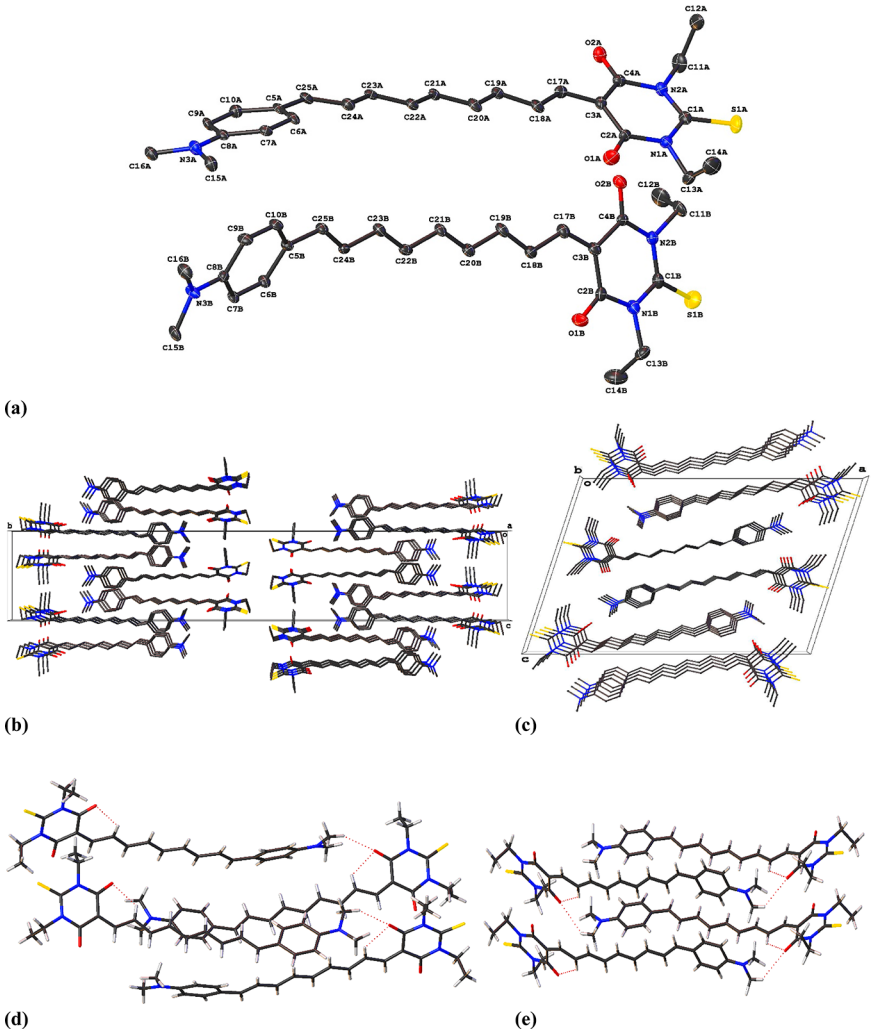

Figure 11. Asymmetric unit of TB[5]α containing two symmetrically independent molecules A and B (hydrogen atoms are omitted) (a), their packing along the *a* axis (b), packing diagram of TB[5]β along the *b* axis (c), hydrogen bonds for TB[5]α (d), and TB[5]β (e).

by A. Gavezzotti.[35,36] Molecular energies and dipole moments characterizing different conformations have been evaluated using quantum chemical approximation. Obtained results (Tables S4 and S5, Supporting Information) demonstrated that polymorphs of TB[1], in spite of differences in molecular conformations, have very close values of dipole moments and lattice energy, so it is possible to suggest that those polymorphs are equally stable. Actually, equal stability of two polymorphs of TB[1] is supported by appearing of two concomitant polymorphs for this compound (see Figure 3). For molecules of polymorphs TB[3], similar dipole moments and close lattice energies have been found that does not allow us to make definite conclusion about the relative stability of polymorphs for this material. For TB[5] polymorphs, based on their lattice energy, it is possible to conclude that TB[5]α is more stable than TB[5] β. However, if we consider the difference in molecular conformation energy for two polymorphs, these polymorphs can be considered almost equally probable. More information about relative stability of polymorphs and their phase transition might be obtained from differential scanning calorimetry (DSC) studies. Such data on powder samples of TB [1], TB[2], and TB[3] are presented in Figure S9 and Table S7, Supporting Information. Presented plots are very similar to the plot describing phase transition for the polymorphic system of sulphapyridine[1] that suggests the possibility of phase transition for all compounds studied including TB[2], for which just one crystal form was found until now.

A known relationship between hyperpolarizability β and bond length alternation (BLA) is commonly used for estimating molecular nonlinear optical properties. The BLA value shows which molecule form is predominant: if the neutral form prevails in the ground state, then $0 < \text{BLA/Å} < 0.11$, zwitterionic form predominance leads to $-0.11 > \text{BLA/Å} > 0$. Equal mixing of the two limiting resonance forms gives BLA and β values of 0, while β is maximal at intermediate BLA values $\pm (0.05 \pm 0.01)$ Å.[41] Selected bond lengths presented in Table 2, Supporting Information revealed that all the molecules possess a pronounced quinoid character of donor groups. BLA values for molecules of TB[1]α, TB[1]β, TB[2], TB[3]α, TB[3]β, TB[5]α (molecule A), TB[5]α (molecule B) and TB[5]β are 0.046, 0.043, 0.033, 0.052, 0.055, 0.076, 0.077, and 0.070 Å, respectively. Thus, BLA for TB[1]α, TB[1]β, TB[3]α, and TB[3]β corresponds to the maximum β value. However, since all the obtained structures have a centrosymmetric space group, the molecules of the unit cell cancel each other out in terms of NLO properties. Thus, using these molecules for nonlinear optical applications, it would be

DOI: 10.1021/acs.cgd.9b00961
Cryst. Growth Des. 2020, 20, 167−177

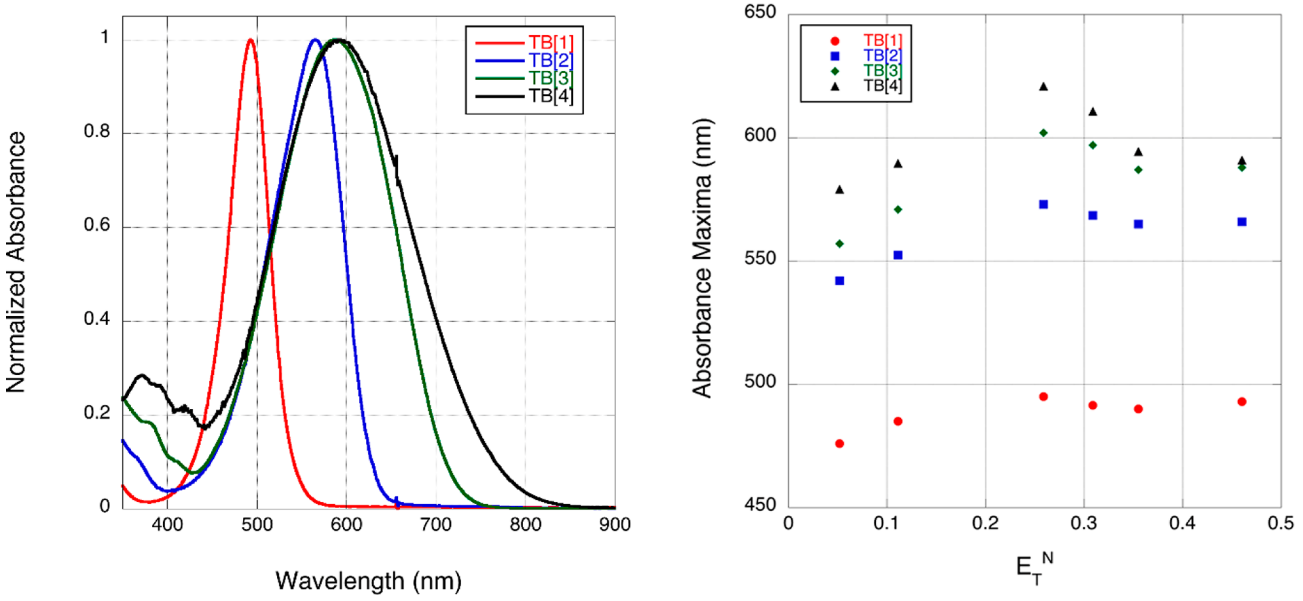

Figure 12. Normalized absorbance spectra of TB[n] series in acetonitrile (left) and solvatochromism of TB[n] series as compared to Reichardt's normalized transition energy scale (right).[43] Solvents from left to right: carbon tetrachloride, benzene, chloroform, dichloromethane, acetone, and acetonitrile. For all series, the absorbance maxima of DMSO was excluded.

possible to incorporate them in the polymer matrix and pole obtained material.

The previously reported polymorph of TB[1]α and its -N(^{n}Bu)$_2$ analogue are known to possess large first hyperpolarizabilities.[38] Despite the fact that TB[1] contains only a single methine unit and, thus, BLA values for both polymorphs are only a rough estimation, structural data are clearly consistent with the noticeable NLO properties of this molecule.

The calculated HOMO/LUMO energies for molecules with crystal geometries and optimized geometries are summarized in Table 4, Supporting Information. According to the correlation results on thermal stability[23] and calculated values of HOMO energies, it is possible to conclude that molecules with longer π-conjugated bridge possess a higher HOMO energy and thus have a higher thermal stability. This suggestion agrees with the results on thermal stability for similar types of compounds with different lengths of π-conjugated bridge.[42]

Studied series of diethylthiobarbituric acid terminated merocyanines shows electronic spectra typical of donor−acceptor chromophores, presenting a charge transfer band which is both strong and quite broad (Figure 12).

The TB[n] series also shows pronounced solvatochromism, which is characterized as inverted.[43] As is shown in Figure 12 and Table 5, Supporting Information, in lower polarity solvents the series exhibits positive solvatochromism, and in higher polarity solvents it reverses to negative solvatochromism. Also, it appears in acetonitrile that the solvatochromic behavior again reverses to positive. As is described by Reichardt,[43] solvatochromism is the result of different solvation of the ground and excited states of a molecule. Solvatochromism is typically described in terms of the effects of increasing solvent polarity on the absorption maxima. Positive solvatochromism occurs when a bathochromic (red) shift in absorbance occurs, while negative solvatochromism occurs when a hypsochromic (blue) shift in absorbance occurs. In terms of energies, positive solvatochromism is the result of the stabilization of the excited state, and negative solvatochromism is due to the stabilization of the ground state of the chromophore. In the case of the TB[n] series, the inverted solvatochromism is likely due to a solvent-induced change in the ground state structure with increasing polarity.[43]

Evidence for the change in ground state structure can be seen by NMR. Vicinal coupling constants in trans-double bonds are typically about 16.5 Hz but can range between 12−24 Hz. The typical coupling constant between two antiperiplanar protons on sp^2 carbons bound by a single bond is about 10 Hz. These typical values can be taken as the extreme values for a bond length alternation approximation.[44]

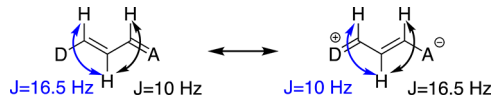

Figure 13. Bond length alternation by NMR spectroscopy.

When measures by crystal structure, the formula for bond length alternation is the average single bond length subtracted by the average double bond length. This formula establishes a positive BLA value for the valence bonding structure and a negative BLA for the charge transfer structure. To keep this same convention, the formula for bond length alternation by NMR, ΔJ to avoid confusion, must be flipped so that the valence bonding structure has a positive ΔJ:

$$\Delta J = \overline{J}_{C=C} - \overline{J}_{C-C}$$

Using this convention, the limiting ΔJ values are 6.5 Hz for the valence bonding structure and −6.5 Hz for the charge transfer contributor.

The solvent dependence of the ΔJ values is indicative of a change in ground state configuration caused by the solvent. Also, of note in Figure 14, the increase in solvent polarity dramatically reduces the overall ΔJ, indicating that the solvent-based stabilization of the charge-transfer state has a major

DOI: 10.1021/acs.cgd.9b00961
Cryst. Growth Des. 2020, 20, 167−177

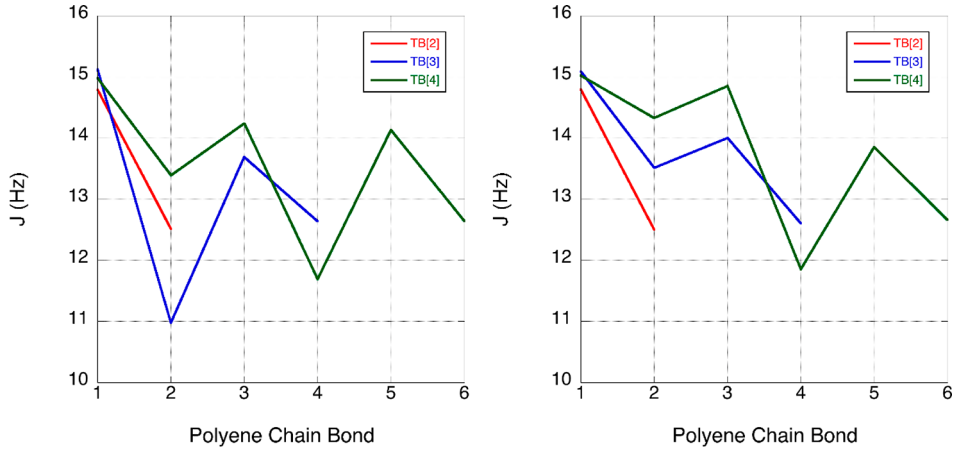

Figure 14. Oscillatory behavior of proton coupling constants along polyene chain from donor end to acceptor end for TB[n] in CD_2Cl_2 (left) and TB[n] in CD_3CN (right).

impact on the electronic structure and solvatochromic behavior of the TB[n] series.

Hyper-Rayleigh scattering measurements showed an increase in β with chain length in all solvents. The results are shown in Figure 15 and summarized in Table 6, Supporting Information. Degradation occurred during the measurements of TB[4] in chloroform and in DMF, which was unable to be mitigated by stirring or a reduction in power.

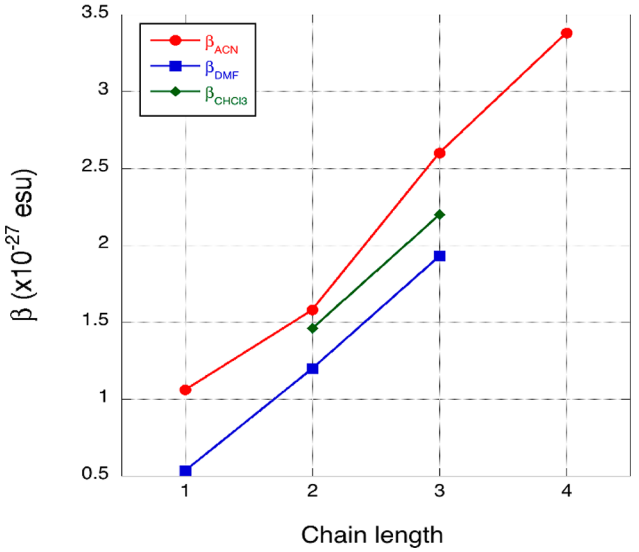

Figure 15. First hyperpolarizability of TB[1]−TB[4] in chloroform, acetonitrile, and *N*,*N*-dimethylformamide as measured by HRS at 900 nm.

CONCLUSIONS

Several crystalline structures of thiobarbituric acid derivatives were obtained from solutions. It was clearly shown that variations of crystal shape for samples obtained from different solvents do not indicate the presence of various polymorphs, and vice versa different polymorphs can be obtained from the same solvent (concomitant polymorphism). For all three pairs of polymorphs, different molecular conformations in crystals caused by different orientation of ethyl groups were found. BLA values for some of these crystals correspond to very high hyperpolarizability values. It was shown that an increase of molecular polarizability is related to an increase of the length of the π-conjugated bridge that was supported by experimental hyper-Rayleigh scattering data. However, because of the centrosymmetric space groups in all these structures, NLO applications of the obtained compounds are possible only in poled matrixes.

ASSOCIATED CONTENT

Supporting Information

The Supporting Information is available free of charge at https://pubs.acs.org/doi/10.1021/acs.cgd.9b00961.

Summary of crystal data and refinement results, selected bond lengths and dihedral angles, hydrogen bonds, calculated HOMO/LUMO, molecular and crystal structure energies, DSC, spectroscopy and hyperpolarizability data (PDF)

Accession Codes

CCDC 1941677−1941683 contain the supplementary crystallographic data for this paper. These data can be obtained free of charge via www.ccdc.cam.ac.uk/data_request/cif, or by emailing data_request@ccdc.cam.ac.uk, or by contacting The Cambridge Crystallographic Data Centre, 12 Union Road, Cambridge CB2 1EZ, UK; fax: +44 1223 336033.

AUTHOR INFORMATION

Corresponding Author

*E-mail: tvtimofeeva@nmhui.edu.

ORCID

Joseph Perry: 0000-0003-1101-7337
Victor N. Khrustalev: 0000-0001-8806-2975
Tatiana V. Timofeeva: 0000-0001-7475-3206

Notes

The authors declare no competing financial interest.

ACKNOWLEDGMENTS

This work was supported by the U.S. National Science Foundation (Grants DMR-1523611 PREM and MRI-1827875) and the RUDN University Program "5-100". We are grateful to Dr. S. Lindeman and Dr. A. Metta for help with data collection and structure solution.

DOI: 10.1021/acs.cgd.9b00961
Cryst. Growth Des. 2020, 20, 167−177

REFERENCES

(1) Bernstein, J. *Polymorphism in Molecular Crystals*; Clarendon Press: Oxford, 2002.
(2) Bernstein, J. *Polymorphism in Molecular Crystals*; Antipin, M. Yu., Timofeeva, T. V.; Eds.; Nauka: Moscow, 2007.
(3) Price, S. L. Predicting crystal structures of organic compounds. *Chem. Soc. Rev.* **2014**, *43*, 2098−2111.
(4) Price, S. L. Is zeroth order crystal structure prediction (CSP_0) coming to maturity? What should we aim for in an ideal crystal structure prediction code? *Faraday Discuss.* **2018**, *211*, 9−30.
(5) Price, S. L. Why don't we find more polymorphs? *Acta Crystallogr., Sect. B: Struct. Sci., Cryst. Eng. Mater.* **2013**, *B69*, 313−328.
(6) Gnutzmann, T.; Nguyen Thi, Y.; Rademann, K.; Emmerling, F. Solvent-Triggered Crystallization of Polymorphs Studied in Situ. *Cryst. Growth Des.* **2014**, *14*, 6445−6450.
(7) Miller, J. M.; Rodriguez-Hornedo, N.; Blackburn, A. C.; Macikenas, D.; Collman, B. M. Solvent Systems for Crystallization and Polymorph Selection. In *Solvent Systems and Their Selection in Pharmaceutics and Biopharmaceutics*; Augustijns, P., Brewster, M. E.; Eds.; Springer, New York, 2007; Biotechnology: Pharmaceutical Aspects, Vol. *VI*.
(8) Guranda, D. T.; Gil'deeva, G. N. Preparation of drug polymorphs (a review). *Pharm. Chem. J.* **2010**, *44*, 254−260.
(9) Raza, K.; Kumar, P.; Ratan, S.; Malik, R.; Arora, S. Polymorphism: The Phenomenon Affecting the Performance of Drugs. *SOJ. Pharm. Pharm. Sci.* **2014**, *1* (2), 10.
(10) Karpinski, P. Polymorphism of Active Pharmaceutical Ingredients. *Chem. Eng. Technol.* **2006**, *29* (2), 233−237.
(11) Ruiz, B.; Coe, B. J.; Gianotti, R.; Gramlich, V.; Jazbinsek, M.; Günter, P. Polymorphism, crystal growth and characterization of an organic nonlinear optical material: DAPSH. *CrystEngComm* **2007**, *9*, 772−776.
(12) Etter, M. C.; Frankenbach, G. M.; Adsmond, D. A. Using Hydrogen Bonds to Design Acentric Organic Materials for Nonlinear Optical Materials. *Molecular Crystals and Liquid Crystals Incorporating Nonlinear Optics.* **1990**, *187* (1), 25−39.
(13) Timofeeva, T. V.; Nesterov, V. N.; Wang, Z.; Clark, R. D.; Antipin, M. Y. Crystalline polymorphs and co-crystals for nonlinear optics. Proc. SPIE 4813, *Crystal Materials for Nonlinear Optical Devices and Microgravity Science*, 2002.
(14) Pan, F.; Bosshard, C.; Wong, M. S.; Serbutoviez, C.; Schenk, K.; Gramlich, V.; Günter, P. Selective Growth of Polymorphs: An Investigation of the Organic Nonlinear Optical Crystal 5-Nitro-2-thiophenecarboxaldehyde-4-methylphenylhydrazone. *Chem. Mater.* **1997**, *9*, 1328−1334.
(15) Timofeeva, T. V.; Nesterov, V. N.; Clark, R. D.; Penn, B.; Frazier, D.; Antipin, M. Y. Systematic study of polymorphism in crystalline non-linear optical materials. *J. Mol. Struct.* **2003**, *647* (1−3), 181−202.
(16) Benmansour, S.; Marchivie, M.; Triki, S.; Gómez-García, C. J. Polymorphism and Metallic Behavior in BEDT-TTF Radical Salts with Polycyano Anions. *Crystals* **2012**, *2*, 306−326.
(17) Yamamoto, H. M.; Hagiwara, M.; Kato, R. New phase of (BEDT-TTF)(TCNQ). *Synth. Met.* **2003**, *133−134*, 449−451.
(18) Mori, T.; Inokuchi, H. Structural and electrical properties of (BEDT-TTF)(TCNQ). *Solid State Commun.* **1986**, *59* (6), 355−359.
(19) Atkinson, M. B. J.; Bwambok, D. K.; Chen, J.; Chopade, P. D.; Thuo, M. M.; Mace, C. R.; Mirica, K. A.; Kumar, A. A.; Myerson, A. S.; Whitesides, G. M. Using Magnetic Levitation to Separate Mixtures of Crystal Polymorphs. *Angew. Chem., Int. Ed.* **2013**, *52*, 10208−10211.
(20) Henderson, J.; Masino, M.; Hatcher, L. E.; Kociok-Köhn, G.; Salzillo, T.; Brillante, A.; Raithby, P. R.; Girlando, A.; Da Como, E. New Polymorphs of Perylene:Tetracyanoquinodimethane Charge Transfer Cocrystals. *Cryst. Growth Des.* **2018**, *18*, 2003−2009.
(21) Marder, S. R.; Beratan, D. N.; Cheng, L. T. Approaches for Optimizing the First Electronic Hyperpolarizability of Conjugated Organic Molecules. *Science* **1991**, *252*, 103−106.
(22) Moylan, C. R.; Twieg, R. J.; Lee, V. Y.; Swanson, S. A.; Betterton, K. M.; Miller, R. D. Nonlinear optical chromophores with large hyperpolarizabilities and enhanced thermal stabilities. *J. Am. Chem. Soc.* **1993**, *115*, 12599−12600.
(23) Figueiredo, L. J. O.; Garrido, F. M. S. Chemometric analysis of nonlinear optical chromophores structure and thermal stability. *J. Mol. Struct.: THEOCHEM* **2001**, *539*, 75−81.
(24) Xu, J.; Guo, B.; Chen, B.; Zhang, Q. A QSPR treatment for the thermal stabilities of second-order NLO chromophore molecules. *J. Mol. Model.* **2005**, *12*, 65−75.
(25) Marder, S. R.; Cheng, L.-T.; Tiemann, B. G.; Friedli, A. C.; Blanchard-Desce, M.; Perry, J. W.; Skindhøj, J. Large First Hyperpolarizabilities in Pus h-Pull Polyenes by Tuning of the Bond Length Alternation and Aromaticity. *Science* **1994**, *263*, 511−514.
(26) Paschoal, D.; Dos Santos, H. F. Computational protocol to predict hyperpolarizabilities of large π-conjugated organic push−pull molecules. *Org. Electron.* **2016**, *28*, 111−117.
(27) Naik, P.; Su, R.; Babu, D. D.; El-Shafei, A.; Adhikari, A. V. Structurally simple D−A-type organic sensitizers for dye-sensitized solar cells: effect of anchoring moieties on the cell performance. *J. Iran. Chem. Soc.* **2017**, *14*, 2457−2466.
(28) Tillotson, J. P.; Bogdanov, G.; Jucov, E. V.; Khrustalev, V. N.; Rigin, S.; Hales, J. M.; Perry, J. W.; Timofeeva, T. V. Synthesis, structure, linear and nonlinear properties of Tricyanofuran−Terminated merocyanine dyes. *J. Mol. Struct.* **2019**, *1189*, 146−154.
(29) Chetina, O. *How to Grow Single Crystals for X-ray Analysis by Solution Crystallisation*; ENOD Press, 2012.
(30) Sheldrick, G. M. *SADABS*, v. 2.03, Bruker/Siemens Area Detector Absorption Correction Program: Bruker AXS: Madison, WI, 2003.
(31) *CrysAlis PRO*, version 171.39.46; Agilent Technologies UK Ltd: Yarnton, Oxfordshire, England, 2018.
(32) Sheldrick, G. M. SHELXT - Integrated space-group and crystal-structure determination. *Acta Crystallogr., Sect. A: Found. Adv.* **2015**, *A71*, 3−8.
(33) Dolomanov, O. V.; Bourhis, L. J.; Gildea, R. J.; Howard, J. A. K.; Puschmann, H. OLEX2: a complete structure solution, refinement and analysis program. *J. Appl. Crystallogr.* **2009**, *42*, 339−341.
(34) Frisch, M. J.; Trucks, G. W.; Schlegel, H. B.; Scuseria, G. E.; Robb, M. A.; Cheeseman, J. R.; Scalmani, G.; Barone, V.; Petersson, G. A.; Nakatsuji, H.; Li, X.; Caricato, M.; Marenich, A. V.; Bloino, J.; Janesko, B. G.; Gomperts, R.; Mennucci, B.; Hratchian, H. P.; Ortiz, J. V.; Izmaylov, A. F.; Sonnenberg, J. L.; Williams-Young, D.; Ding, F.; Lipparini, F.; Egidi, F.; Goings, J.; Peng, B.; Petrone, A.; Henderson, T.; Ranasinghe, D.; Zakrzewski, V. G.; Gao, J.; Rega, N.; Zheng, G.; Liang, W.; Hada, M.; Ehara, M.; Toyota, K.; Fukuda, R.; Hasegawa, J.; Ishida, M.; Nakajima, T.; Honda, Y.; Kitao, O.; Nakai, H.; Vreven, T.; Throssell, K.; Montgomery, J. A., Jr.; Peralta, J. E.; Ogliaro, F.; Bearpark, M. J.; Heyd, J. J.; Brothers, E. N.; Kudin, K. N.; Staroverov, V. N.; Keith, T. A.; Kobayashi, R.; Normand, J.; Raghavachari, K.; Rendell, A. P.; Burant, J. C.; Iyengar, S. S.; Tomasi, J.; Cossi, M.; Millam, J. M.; Klene, M.; Adamo, C.; Cammi, R.; Ochterski, J. W.; Martin, R. L.; Morokuma, K.; Farkas, O.; Foresman, J. B.; Fox, D. J. *Gaussian 16*, Revision B.01; Gaussian, Inc.: Wallingford, CT, 2016.
(35) Gavezzotti, A. Efficient computer modeling of organic materials. The atom−atom, Coulomb−London−Pauli (AA-CLP) model for intermolecular electrostatic-polarization, dispersion and repulsion energies. *New J. Chem.* **2011**, *35*, 1360−1368.
(36) Gavezzotti, A. Equilibrium structure and dynamics of organic crystals by Monte Carlo simulation: critical assessment of force fields and comparison with static packing analysis. *New J. Chem.* **2013**, *37*, 2110−2119.
(37) Campo, J.; Desmet, F.; Wenseleers, W.; Goovaerts, E. Highly sensitive setup for tunable wavelength hyper-Rayleigh scattering with parallel detection and calibration data for various solvents. *Opt. Express* **2009**, *17* (6), 4587−4604.
(38) Adamson, J.; Coe, B. J.; Grassam, H. L.; Jeffery, J. C.; Coles, S. J.; Hursthouse, M. B. Reactions of 1,3-diethyl-2-thiobarbituric acid with aldehydes: formation of arylbis(1,3-diethyl-2-thiobarbitur-5-

DOI: 10.1021/acs.cgd.9b00961
Cryst. Growth Des. 2020, 20, 167−177

yl)methanes and crystallographic evidence for ground state polarisation in 1,3-diethyl-5-[4-(dimethylamino)benzylidene]-2-thiobarbituric acid. *J. Chem. Soc., Perkin Trans. 1* **1999**, *1*, 2483−2488.
(39) Bernstein, J.; Davey, R. J.; Henck, J. O. Concomitant Polymorphs. *Angew. Chem., Int. Ed.* **1999**, *38* (23), 3440−3461.
(40) Macrae, C. F.; Bruno, I. J.; Chisholm, J. A.; Edgington, P. R.; McCabe, P.; Pidcock, E.; Rodriguez-Monge, L.; Taylor, R.; van de Streek, J.; Wood, P. A. Mercury CSD 2.0 - new features for the visualization and investigation of crystal structures. *J. Appl. Crystallogr.* **2008**, *41*, 466−470.
(41) Blanchard-Desce, M.; Alain, V.; Bedworth, P. V.; Marder, S. R.; Fort, A.; Runser, C.; Barzoukas, M.; Lebus, S.; Wortmann, R. Large Quadratic Hyperpolarizabilities with Donor−Acceptor Polyenes Exhibiting Optimum Bond Length Alternation: Correlation Between Structure and Hyperpolarizability. *Chem. - Eur. J.* **1997**, *3*, 1091−1104.
(42) Lindsay, G. A.; Henry, R. A.; Yee, R. Y.; Chafin, A. P.; Seltzer, M. D.; Hill, R.; Knoesen, A. Second harmonic generation from new dyes in polymer films. *Proc. SPIE* **1994**, *2143*, 88−98.
(43) Reichardt, C. Solvatochromic Dyes as Solvent Polarity Indicators. *Chem. Rev.* **1994**, *94* (8), 2319−2358.
(44) Parthasarathy, V.; Pandey, R.; Das, P. K.; Castet, F.; Blanchard-Desce, M. Linear and Nonlinear Optical Properties of Tricyanopropylidene-Based Merocyanine Dyes: Synergistic Experimental and Theoretical Investigations. *ChemPhysChem* **2018**, *19* (2), 187−197.

DOI: 10.1021/acs.cgd.9b00961
Cryst. Growth Des. 2020, 20, 167−177